STEM CELLS TRANSLATIONAL MEDICINE®

EMBRYONIC STEM CELLS/INDUCED PLURIPOTENT STEM (iPS) CELLS

Chemically Induced Specification of Retinal Ganglion Cells From Human Embryonic and Induced Pluripotent Stem Cells

HAMIDREZA RIAZIFAR,[a] YOUSHENG JIA,[b] JING CHEN,[c] GARY LYNCH,[b,d] TAOSHENG HUANG[a,c,e,f,g]

Key Words. Retinal ganglion cells • Induced pluripotent stem cells • Embryonic stem cells • Differentiation • Notch signaling

ABSTRACT

The loss of retinal ganglion cells (RGCs) is the primary pathological change for many retinal degenerative diseases. Although there is currently no effective treatment for this group of diseases, cell transplantation to replace lost RGCs holds great potential. However, for the development of cell replacement therapy, better understanding of the molecular details involved in differentiating stem cells into RGCs is essential. In this study, a novel, stepwise chemical protocol is described for the differentiation of human embryonic stem cells and induced pluripotent stem cells into functional RGCs. Briefly, stem cells were differentiated into neural rosettes, which were then cultured with the Notch inhibitor *N*-[*N*-(3,5-difluorophenacetyl)-L-alanyl]-*S*-phenylglycine *t*-butyl ester (DAPT). The expression of neural and RGC markers (BRN3A, BRN3B, ATOH7/Math5, γ-synuclein, Islet-1, and THY-1) was examined. Approximately 30% of the cell population obtained expressed the neuronal marker TUJ1 as well the RGC markers. Moreover, the differentiated RGCs generated action potentials and exhibited both spontaneous and evoked excitatory postsynaptic currents, indicating that functional and mature RGCs were generated. In combination, these data demonstrate that a single chemical (DAPT) can induce PAX6/RX-positive stem cells to undergo differentiation into functional RGCs. STEM CELLS TRANSLATIONAL MEDICINE *2014;3:424–432*

[a]Department of Pediatrics, Division of Human Genetics, [b]Department of Anatomy and Neurobiology, [d]Department of Psychiatry and Human Behavior, [e]MitoMed Molecular Diagnostic Laboratory, Department of Pathology, [f]Department of Developmental and Cell Biology, and [g]Department of Ophthalmology, University of California, Irvine, Irvine, California, USA; [c]Division of Human Genetics, Cincinnati Children's Hospital Medical Center, Cincinnati, Ohio, USA

Correspondence: Taosheng Huang, M.D., Ph.D., Division of Human Genetics, Cincinnati Children's Hospital Medical Center, 3333 Burnet Avenue, Building R, Room 1027, MLC 7016, Cincinnati, Ohio 45229, USA. Telephone: 949-824-9346; E-Mail: Taosheng.Huang@cchmc.org

Received August 19, 2013; accepted for publication November 4, 2013; first published online in SCTM *EXPRESS* February 3, 2014.

1066-5099/2014/$20.00/0

http://dx.doi.org/10.5966/sctm.2013-0147

INTRODUCTION

A diverse group of vision disorders are caused by degeneration of the retina. These diseases, such as glaucoma and optical atrophy disorders, affect millions of people worldwide with varying degrees of irreversible vision loss resulting from the loss of retinal ganglion cells (RGCs). In glaucoma, RGC loss is the primary pathological change and can occur at any age. Glaucoma is the second leading cause of blindness in the world [1]. Approximately 10% of blindness in the United States is associated with glaucoma. It is estimated that approximately 4 million Americans suffer from glaucoma, but only half of those affected have been diagnosed. The cause of glaucoma can be genetic or nongenetic. Currently, there is no cure for glaucoma, and medications and surgical intervention can only slow down the progression of vision loss. Unfortunately, approximately 10% of patients with glaucoma will lose their vision even if treated appropriately [2].

RGC death is also implicated in optic atrophy disorders such as dominant optic atrophy (DOA) and Leber's hereditary optic atrophy (LHON). DOA is marked by progressive bilateral loss of visual acuity, visual field deficits, and abnormal color vision [3–6]. LHON results in a sudden onset of visual loss and appears at a later age (18–35 years). In addition, LHON is maternally inherited and is caused by mutations in the mitochondrial genome [7]. During the atrophic phase, it is difficult to distinguish LHON from DOA without a family history. Currently, there are no effective treatments for all of these degenerative retinal diseases resulting from RGC loss [8, 9]. However, human embryonic stem cells (hESCs) and induced pluripotent stem (iPS) cells provide promising therapeutic possibilities. Therefore, differentiation of hESCs or iPS cells into RGCs has been actively studied. However, an efficient and simplified method for RGC differentiation is lacking. A major problem facing this strategy is the difficulty of transforming stem cells into fully functional RGCs. Because ethical issues have complicated the ability to use hESCs for therapeutic purposes, recent work has been focused on the possibility of using iPS cells, which can be obtained from patient-matched adult cells, to generate replacements for the RGCs that are lost in retinal degenerative diseases [10–12].

The RGC differentiation process is complicated and is regulated by many intrinsic and extrinsic factors. Many transcription factors are critical for differentiation of stem cells into RCGs. A high level of PAX6 expression has been shown in the mouse to be required for the activation of Math5 (homologous to ATOH7 in humans), a basic helix-loop-helix (bHLH) transcription factor

that plays an important role in RGC specification and differentiation [13]. Gain and loss of function studies have demonstrated that ATOH7/Math5 is essential for the development of the RGC lineage [14–17]. Recent studies have further shown that the deletion of the remote enhancer of human ATOH7/Math5 disrupts retinal generation and causes nonsyndromic congenital retinal detachment [16]. Moreover, mutations in Math5 disrupt the generation of RGCs [14]. Several transcription factors, including BRN3a, BRN3b, and BRN3c are translated after Math5 is expressed, suggesting that Math5 regulates the BRN3 family [18]. All of these factors have been used as the markers of RGCs.

To determine whether stem cells have been successfully differentiated into RGCs, markers that are specific to these specialized neurons have to be examined. Early markers for RGCs include RX, a homeobox-containing protein that plays a critical role in normal eye development, and PAX6, which is commonly used as a marker for neuroepithelial differentiation [19]. Shortly after completing their terminal mitosis, ~80% of RGC precursor cells express the POU-domain proteins BRN3b and BRN3a [20–22]. Thus, the expression levels of BRN3a and BRN3b can be used to indicate the differentiation of stem cells into RGCs. Islet-1 is a LIM-homeodomain protein that is expressed in RGCs during retinal genesis, particularly in biopolar, interneural, and amacrine cells [23]. γ-Synuclein is highly expressed in proximity to BRN3a in the axons and cytoplasm of RGCs. Accordingly, coexpression of BRN3a and γ-synuclein is also considered a marker of RGCs [24]. Finally, the cell surface protein THY-1/CD90, originally discovered as a thymocyte antigen, can also serve as an RGC marker [25].

During RGC development, the activation of Notch signaling has been found to prevent RGC differentiation [26]. Notch activity has been shown in the mouse to be downregulated just prior to the differentiation of RGCs during normal eye development, and Notch signaling is inhibited by *N*-[*N*-(3,5-difluorophenacetyl)-L-alanyl]-*S*-phenylglycine *t*-butyl ester (DAPT) [26, 27]. This discovery of the role of Notch signaling in RGC differentiation prompted us to develop the protocol for the retina-specific differentiation of stem cells or iPS cells presented in this paper [19, 28–30]. We hypothesized that hESCs and iPS cells expressing a high level of PAX6 can be induced into functional RGCs when notch signaling is inhibited. To test this hypothesis in human embryonic stem (ES) cell and iPS cell models, a two-step approach was designed in which human ES cells and iPS cells were first differentiated into $PAX6^+$ and RAX^+ (retinal Rx) neural rosettes. We then found that the Notch signaling inhibitor DAPT is sufficient to induce neural rosettes into functional RGCs.

Materials and Methods

Culture of hESCs and iPS Cells

Clinical-grade hESCs (H9) were purchased from the WiCell Research Institute (Madison, WI, http://www.wicell.org), and iPS cells were derived from skin fibroblast cells obtained by a needle punch biopsy with an approved institutional review board protocol from the University of California, Irvine. Following the biopsy, the skin fibroblast cells were cultured and infected with retroviruses expressing the human transcription factors OCT4, SOX2, KLF4, and c-MYC to induce pluripotency, as described previously [31]. Multiple iPS cell colonies were generated and examined for the presence of iPS cell markers and the ability to form teratomas. The iPS cells and hESCs were maintained in human embryonic stem (hES) medium (Knockout Dulbecco's modified Eagle's medium/Nutrient Mixture F-12 [DMEM/F-12] containing 20% knockout serum replacement, 1 mM GlutaMAX (Life Technologies, Grand Island, NY, http://www.lifetechnologies.com), 1 mM nonessential amino acids, 0.1 mM 2-mercaptoethanol, 1 mM penicillin, and 1 mM streptomycin) supplemented with 10 ng/ml basic fibroblast growth factor (bFGF; Millipore, Billerica, MA, http://www.millipore.com) and grown on a feeder layer of mitotic-inactivated primary mouse embryo fibroblasts (PMEFs). After the iPS cells and hESCs reached confluence, the medium was removed, the cells were rinsed with phosphate-buffered saline (PBS), collagenase type IV (1 mg/ml) was added (1 ml per well of a six-well plate), and the cells were incubated at 37°C. After 15 minutes, the collagenase was removed, and hES medium was added (1 ml per well). The cells were scraped with a 5-ml pipette, centrifuged at 1,000*g* for 3 minutes, dissociated into small clumps, and plated on fresh PMEFs.

Differentiation of hESCs and iPS Cells

On reaching confluence, cells were scraped into small aggregates and transferred to nonadherent plates (six-well plates; Nunc, Rochester, NY, http://www.nuncbrand.com) in hES media without bFGF for 1 week to generate embryoid bodies. The embryoid bodies were transferred to gelatin-pretreated plates and cultured in hES medium containing 10% fetal bovine serum (FBS). Neural rosettes appeared after several days. One week later, the neural rosettes were mechanically lifted with a syringe needle and a pipette tip and grown in suspension in hES medium containing 10% FBS and 10 μM DAPT (Calbiochem, San Diego, CA, http://www.emdbiosciences.com) for 5 days to allow the formation of neurospheres. The neurospheres were then transferred to laminin-coated plates. The medium and fresh DAPT were renewed every other day. On day 40 following the start of differentiation, the cells were fixed with 4% paraformaldehyde and examined by immunofluorescence (IF).

IF Assays

Cells were washed with PBS, then fixed with 4% paraformaldehyde for 10 minutes at room temperature. IF was performed as described previously [32, 33]. Briefly, after two washes with PBS, cells were incubated with blocking buffer (10% goat serum and 0.3% Triton X-100 in PBS) for 1 hour. Primary antibodies were diluted in blocking buffer and then added to the cells for 1 hour at room temperature. The primary antibodies and dilution are shown in Table 1. The cells were then subjected to three 5-minute washes with PBS and incubated with secondary antibodies diluted in blocking buffer containing DAPI (4′,6-diamidino-2-phenylindole; 1:400) for 1 hour at room temperature. The following secondary antibodies were used: Alexa Fluor 488 goat anti-rabbit IgG, Alexa Fluor 594 goat anti-rabbit IgG, Alexa Fluor 488 goat anti-mouse IgG, and Alexa Fluor 594 goat anti-mouse IgG. After three 5-minute washes with PBS, the cells were visualized with a Nikon Ti Microscope (Nikon, Tokyo, Japan, http://www.nikon.com) at $\times$10 and $\times$20 magnifications and analyzed with the NIS-Elements software (Nikon). For quantification of differentiation efficiency, multiple random images were taken from different parts of plate, and then the cells were counted using ImageJ software for quantification analysis. The *p* value was calculated using the Student *t* test, if applied.

Table 1. Primary antibody information

Antibody
Rabbit anti-human γ-synuclein (1:200; GeneTex, Irvine, CA, http://www.genetex.com)
Rabbit anti-human TUJ1 (1:100; Fitzgerald Industries International, Acton, MA, http://www.fitzgerald-fii.com)
Mouse anti-human Islet-1 (5 μg/ml; Developmental Studies Hybridoma Bank, University of Iowa, Iowa City, IA, http://dshb.biology.uiowa.edu/)
Mouse anti-human BRN3a (1:50; Santa Cruz Biotechnology Inc., Santa Cruz, CA, http://www.scbt.com)
Rabbit anti-human ZO-1 (1:300; Invitrogen, Camarillo, CA, http://www.invitrogen.com)
Rabbit anti-human Pax6 (1:200; Covance, San Diego, CA, http://www.covance.com)
Mouse anti-human Retinal RX (1:200; Santa Cruz Biotechnology)
Rabbit anti-human Nanog (1:100; Epitomics, Burlingame, CA, http://www.epitomics.com)
Rabbit anti-human SSEA-4(1:100; Novus Biologicals, Littleton, CO, http://www.novusbio.com)
Mouse anti-mouse THY-1 (1:50; GeneTex)
Rabbit anti-human THY-1 (1:100; GeneTex)

The tissue sections were analyzed by immunohistochemistry, as described previously [34]. Briefly, the frozen section slides were first placed into HistoVT One solution (Nacalai USA, Inc., San Diego, CA, http://www.nacalaiusa.com) and incubated at 70°C for 20 minutes to complete the antigen-retrieval step and then washed with PBS three times. The slides were blocked in a buffer containing 10% serum (supplemented with 0.3% Triton X-100 when necessary) in PBS for 1.5 hours. The primary antibodies were diluted in the same blocking buffer and incubated with the slides at 4°C overnight. The following day, the slides were washed three times with PBS and incubated with secondary antibodies with DAPI in blocking buffer for 1 hour at room temperature. Following three PBS washes, the slides were mounted with VectaMount (Vector Laboratories, Burlingame, CA, http://www.vectorlabs.com) and glass coverslips and visualized with a Nikon Ti microscope.

Quantitative Polymerase Chain Reaction Assays

RNA was isolated and purified using the RNeasy Plus Mini Kit (Qiagen, Hilden, Germany, http://www.qiagen.com) according to the manufacturer's recommendations. SYBR Green polymerase chain reaction (PCR) was performed in triplicate for each primer set using an ABI Prism 7900HT Sequence Detection System (Applied Biosystems, Foster City, CA, http://www.appliedbiosystems.com), as described previously [32]. Negative-control reverse transcription-PCR (RT-PCR) was included to ensure the absence of DNA contamination. The primers were designed to span introns or to target exon junctions. To ensure the specificity of the PCR assays performed, melting curve analyses were performed at the end of each reaction. The resulting gene expression data were normalized to glyceraldehyde-3-phosphate dehydrogenase and then analyzed with the $2^{\Delta\Delta Ct}$ method, as described previously [32]. The following primers were used for the analysis of ATOH7/Math5: forward, 5′- ACG CAG GGT TCC CCA GT -3′; reverse, 5′- GCG GCC GAA GTG CTC ACA GT -3′. The following primers were used for the analysis of BRN3b: forward, 5′- ACC CCA TGC ACC AAG CAG CG -3′; reverse, 5′- TGC TTG AAG CGC TCG GCG AA -3′.

Electrophysiological Analysis of RGCs

Electrophysiological experiments were performed, as described previously [35]. The cell culture medium was replaced with artificial cerebrospinal fluid containing 124 mM sodium chloride, 3 mM potassium chloride, 1.25 mM monopotassium phosphate, 3.4 mM calcium chloride, 2.5 mM magnesium sulfate, 26 mM sodium bicarbonate, and 10 mM D-glucose (pH 7.3). To assess whether the axons were capable of triggering antidromic spikes, CNQX (20 μM) was added to the medium. Whole-cell current-clamp recordings were obtained with an Axopatch 200A amplifier (Molecular Devices, Sunnyvale, CA, http://www.moleculardevices.com). The data were filtered at 2 kHz, digitized at 1–5 kHz, and analyzed offline with the following programs: Mini Analysis (Synaptosoft, Decatur, GA, http://www.synaptosoft.com), Origin (OriginLab, Northampton, MA, http://www.originlab.com/), and pCLAMP 7 (Axon Instruments/Molecular Devices Corp., Union City, CA, http://www.moleculardevices.com). Depolarizing currents intended to induce action potentials were delivered at 0.05 mA for 1 ms. Stimulation pulses were delivered with a bipolar metal electrode to axon bundles at sites located more than 200 μm from the edges of the cell colonies.

RESULTS

Differentiation of hESCs Into Neural Rosettes

To induce differentiation into neural rosettes, hESCs were incubated in hES medium without bFGF for 1 week. The resulting rosette-like structure was analyzed by IF for the expression of the retinal progenitor cell (RPC) markers RX and PAX6 and the tight junction protein ZO-1 [36]. Typical radial cell morphology was observed after 1 week in culture, and the expression of RX and PAX6 was detectable by IF. Figure 1A shows immunostaining of RX and PAX6. Furthermore, ZO-1 localized to the apical lumens of the structures (Fig. 1B). These data confirm that this protocol generated characteristic neural rosettes.

Differentiated hESCs Express RGC Markers

In order to differentiate the neural rosette into RGCs, we tested the effects of various culture conditions. In this experiment, the neural rosette colonies were maintained in either an adherent or a suspension culture with two different media. In the adherent cultures, the neural rosettes were maintained in the original plates and treated with DAPT for 4 weeks. In the suspension culture condition, neural rosettes were lifted up to form neurospheres and incubated for 5 days in the presence of DAPT. We found only the suspension culture condition allowed us to further differentiate the cells into the structure with long fibers. For different media, DMEM/F-12 supplemented with B27 and DAPT (DMEM/F-12+B27) and hESC medium supplemented with FBS and DAPT (hES/FBS) were tested. After 3 weeks of culture, expression of the RGC marker BRN3a was examined by IF. A significant number of BRN3a-positive cells were observed in both DMEM/F-12+B27 (Fig. 1C) and hES/FBS (Fig. 1D). We then quantified BRN3a-positive cells to determine which medium worked better. In a comparison of DMEM/F-12+B27 medium and hES/FBS medium, hES/FBS medium was superior. As shown in Figure 1E, hESCs in hES/FBS culture medium in the presence of DAPT yielded a significantly higher percentage of BRN3a-positive cells (53% ± 5%) than the DMEM/F-12+B27 culture condition (20% ± 1.0%) (p = .007). The experiment was repeated three

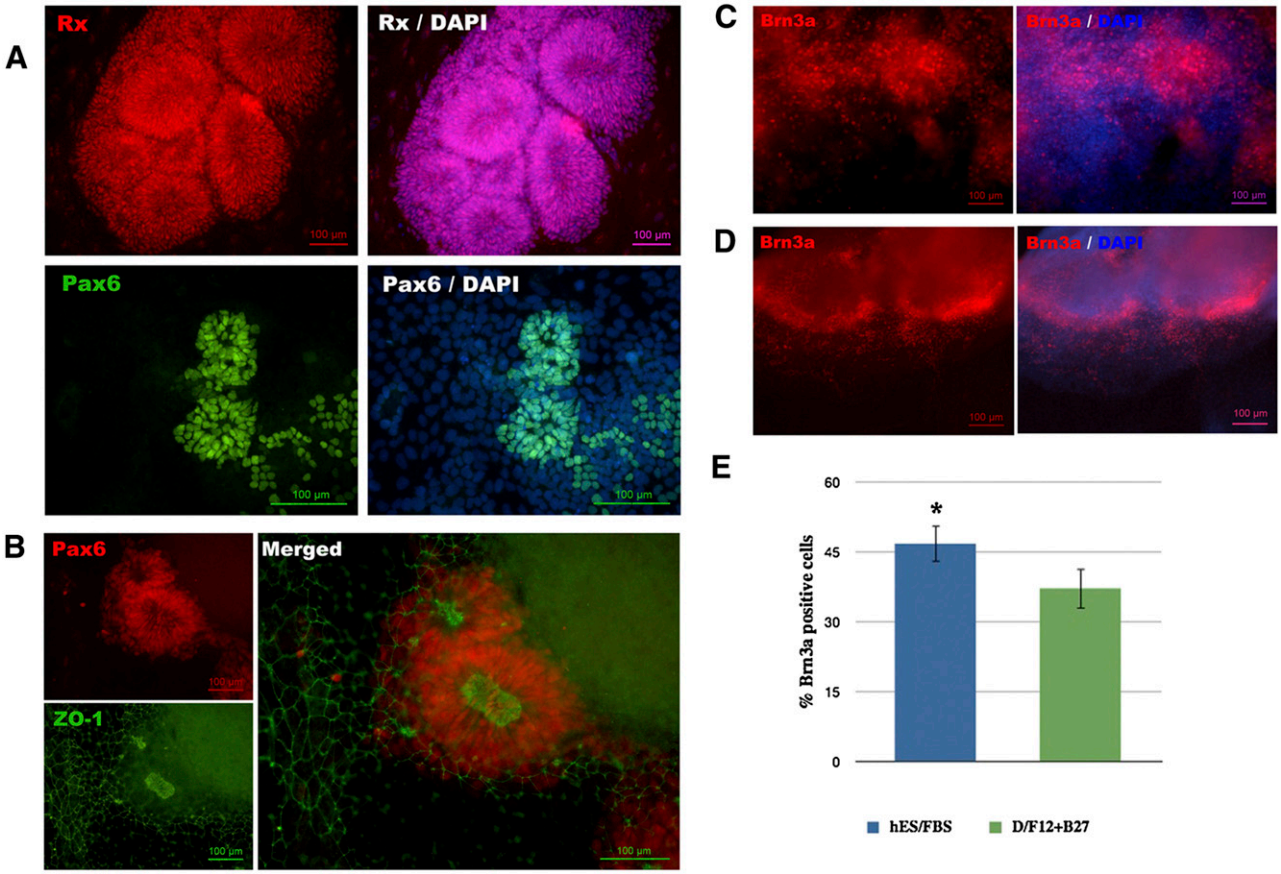

Figure 1. Differentiation of stem cells into neural rosettes. **(A, B):** Human embryonic stem cells (hESCs) and induced pluripotent stem cells were differentiated into neural rosettes. On day 14, the expression levels of RX, PAX6, and ZO-1 were examined in neural rosettes by immunofluorescence, and RX and PAX6 were detected at high levels. The differentiation efficiency of two different culture media was evaluated based on BRN3A expression detected by immunostaining. **(C):** BRN3a+ cells after culturing neural rosettes as neurospheres for 5 days followed by 3 weeks of culture in hES/FBS. **(D):** BRN3a+ cells after neural rosettes were cultured as neurospheres for 5 days followed by 3 weeks in F-12/B27 medium with *N*-[*N*-(3,5-difluorophenacetyl)-L-alanyl]-*S*-phenylglycine *t*-butyl ester (DAPT). **(E):** Comparison of hES/FBS and DMEM/F12+B27. The total number of BRN3a-positive colonies for the hES line in two different medium (hES/FBS and DMEM/F12+B27) were counted after 3 weeks of culture. For each group, eight random images were taken from different parts of the plate. The number of positive cells was normalized with the number of cells. hESCs in hES/FBS culture medium yielded a significantly higher percentage of BRN3a-positive colonies (53% $\pm$ 5%) than DMEM/F-12+B27 culture condition (20% $\pm$ 1.0%) (p = .007). Scale bars = 100 μm. Abbreviations: DAPI, 4′,6-diamidino-2-phenylindole; D/F12+B27, Dulbecco's modified Eagle's medium/Nutrient Mix F-12 supplemented with B27 and DAPT; DAPT, *N*-[*N*-(3,5-difluorophenacetyl)-L-alanyl]-*S*-phenylglycine *t*-butyl ester; hES/FBS, human embryonic stem cell medium supplemented with fetal bovine serum and DAPT.

times, and we produced very similar results. Consequently, hES/FBS culture medium was chosen for all other experiments.

To assess whether the hESCs could differentiated into RGCs, the colonies continued to be cultured, as shown in Figure 2A, and stained for the neuron-specific marker TUJ1 (βIII tubulin) and RGC markers. As shown in Figure 2, after 26-day culture in the presence of DAPT, the differentiated hESCs exhibited long processes (more than 2 cm) (Fig. 2B) and expressed RGC markers BRN3a (Fig. 2B), Islet-1 (Fig. 2C), Thy-1 (Fig. 2D) γ-synuclein (Fig. 2E). Colocalization of BRN3a and γ-synuclein was also analyzed and observed in the differentiated hESC colonies (Fig. 2E). Furthermore, the Islet-1-positive and BRN3a-positive cells aggregated and formed grape-like clusters that connected to one another through elongated fibers, suggesting that interactions existed between cell groups. The specificity of each antibody was confirmed with the retinal tissues. We stained retinal sections with anti-BRN3a, anti-γ-synuclein, and anti-THY-1 antibody. Thy-1, BRN3a, and γ-synuclein were observed only in the RGC layer (supplemental online Fig. 1). To quantify the differentiation efficiency, we attempted to perform fluorescence-activated cell sorting. Stem cells are grown in clusters, and after differentiation, it was even more difficult to disassociate into a single cell suspension for this analysis. For this reason, we performed cell counting with ImageJ software. The percentage of hESCs positive for RGC markers in the hES/FBS culture condition with DAPT was tested. RGC markers BRN3a, γ-synuclein, Islet-1, and Thy-1 were examined. Five random fields were chosen, and a total of 1,536 cells were counted. Approximately 20%–30% of cells are RGC marker positive (22.36% $\pm$ 2.30%) (n = 3).

We then attempted to examine the expression of ATOH7/Math5 by IF; however, we found that neither the commercially available anti-human ATOH7/Math5 antibody nor the BRN3b antibody provided sufficient specificity. Consequently, the level of ATOH7 and BRN3b expression was assessed by RT-PCR. As shown in Figure 2F (left panel), ATOH7Math5 expression was increased 110-fold in the differentiated hESCs over the control, and the

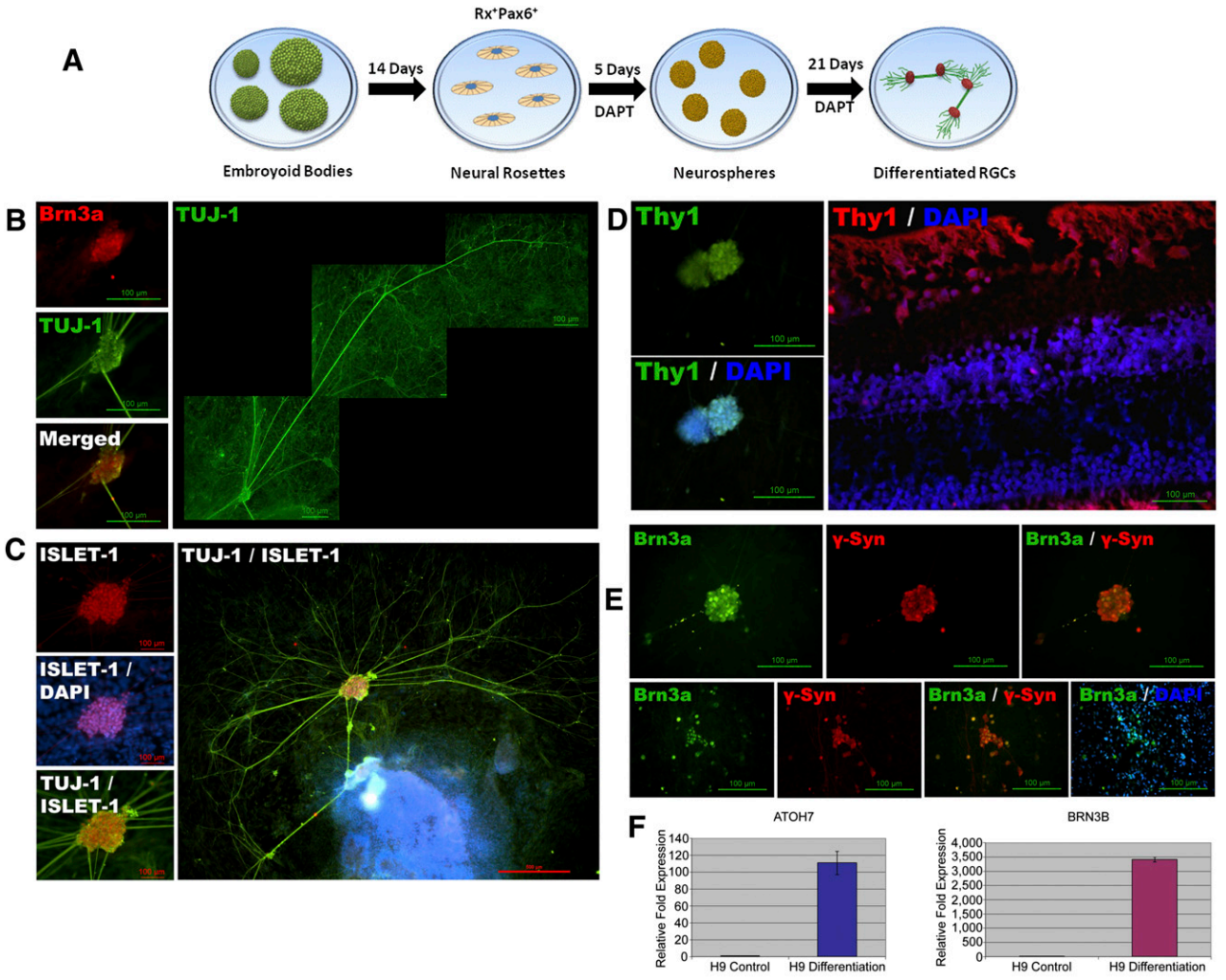

Figure 2. Differentiated human embryonic stem cells (hESCs) are positive for RGC markers. **(A):** Schematic diagram of the procedure used to differentiate hESCs into RGCs. **(B):** Expression of the neuronal marker TUJ1 and the RGC marker BRN3a following application of a stepwise protocol for differentiation of hESCs. **(C):** Expression of the RGC marker Islet-1 following application of a stepwise protocol for differentiation of hESCs. **(D):** THY-1 expression was examined with immunofluorescence (left). **(E):** High-level expression of γ-synuclein in differentiated hESCs. Coexpression of the RGC markers γ-synuclein and BRN3a in differentiated hESCs. **(F):** Quantitative reverse transcription polymerase chain reaction analysis of ATOH7/Math5 and BRN3B in differentiated hESCs. Following differentiation of hESCs according to the stepwise protocol, the mRNA levels of the RGC markers ATOH7/Math5 and BRN3B increased dramatically. Compared with the controls, the level of ATOH7/Math5 increased 110-fold, and the level of BRN3B increased 3,411-fold. Scale bars = 500 μm (**[C]**, right panel) and 100 μm (all other images). Abbreviations: γ-Syn, γ-synuclein; DAPI, 4′,6-diamidino-2-phenylindole; H9, human embryonic stem cell line H9; RGC; retinal ganglion cell.

BRN3b levels were increased by 3,411-fold in the differentiated hESCs after differentiation over the control (Fig. 2F, right panel). Together, these data indicate that the protocol described in this paper efficiently generated RGCs from hESCs.

Expression of RGC Markers in Differentiated Human iPS Cells

Before we differentiated human iPS cell, the iPS cell colonies were first tested by IF for the expression of the stem cell-specific markers NANOG and SSEA-4 (Fig. 3A). Teratoma formation assays were also performed and confirmed the iPS colonies' obtained pluripotency (Fig. 3B). The iPS cells were then differentiated with the protocol described previously for the hESCs. The expression patterns of BRN3a, γ-synuclein, and Islet-1 in the differentiated human iPS cells were similar to those observed in the differentiated hESCs; for example, a majority of the cells were positive for TUJ1, Islet-1 (Figs. 3C, 4B), γ-synuclein (Figs. 3D, 4D), Thy-1 (Fig. 4C). Long fiber bundles, up to 10 μm in diameter, were present and expressed both Islet-1 and TUJ1 (Fig. 3C). The differentiated human iPS cells formed grape-like structures similar to those formed by the hESCs (Fig. 4A, 4B). To quantify the differentiation efficiency, the percentage of iPS cells positive for RGC markers in the hES/FBS condition in the presence of DAPT was also analyzed. The markers BRN3a, γ-synuclein, Islet-1, and Thy-1 were examined. Five random fields were also used, and a total of 1,845 cells were counted with ImageJ software. Overall, 20%–30% cells were RGC marker positive (27.836% ± 2.56%). ATOH7Math5 and BRN3B expression levels were also tested by RT-PCR and increased 857-fold and 6,024-fold, respectively, after differentiation (Fig. 4E). In combination, these data suggest that this novel protocol is very efficient for deriving RGCs from both hESCs and human iPS cells.

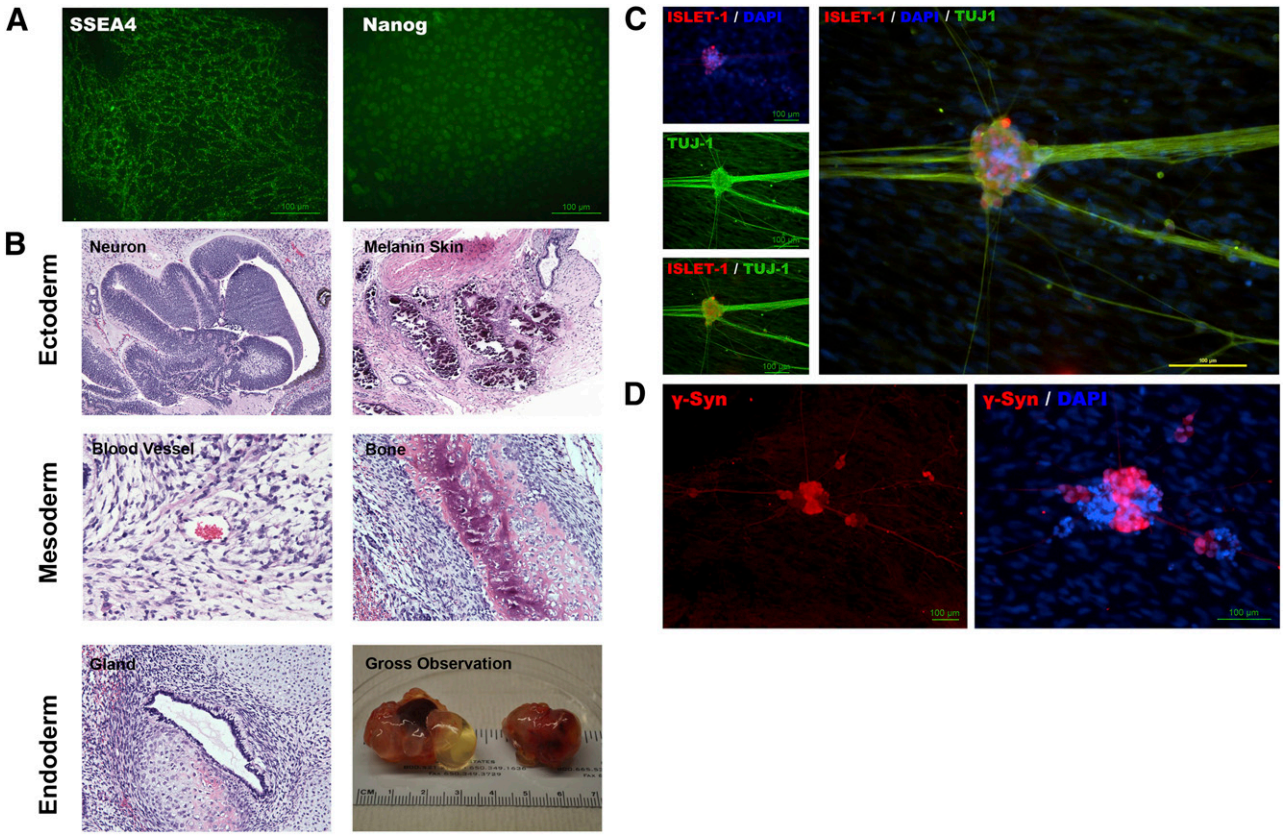

Figure 3. Characterization of induced pluripotent stem (iPS) cells generated from human fibroblasts. **(A):** Characterization of the generated iPS cells in terms of pluripotency markers NANOG (right) and SSEA-4 (left). **(B):** Hematoxylin and eosin staining of iPS cell-derived teratomas shows three germ layers of differentiation: endoderm (gland), mesoderm (blood vessel, bone), and ectoderm (neuron, skin). Examples of dissected teratomas are shown: kidney capsule (left) and testis (right). iPS cells were derived from skin fibroblast cells that were obtained from a needle punch biopsy. The cells were cultured and subsequently infected with a retrovirus expressing OCT4, SOX2, KLF4, and c-MYC. Multiple iPS cell colonies were generated and maintained in hESC medium containing 10 ng/ml basic fibroblast growth factor on a layer of mitotic-inactivated primary mouse embryo fibroblasts cells. **(C):** Expression of the retinal ganglion cell marker Islet-1 (red) and TUJ1 (green). The differentiated cells exhibited fasciculated axons and thick fibers. **(D):** High expression of γ-synuclein in differentiated human iPS cells. Scale bars = 100 μm. Abbreviations: γ-Syn, γ-synuclein; DAPI, 4′,6-diamidino-2-phenylindole.

Differentiated iPS Cells Function as Neurons in Electrophysiological Tests

We next used conventional whole-cell recording methods to determine whether the differentiated iPS cells could function as mature neurons when maintained in artificial cerebrospinal fluid [35]. As shown in Figure 4F, the resting membrane potential was approximately −50 mV, and short depolarizing pulses (0.05 mA) triggered action potentials of 1–2 mV in duration, with a peak amplitude exceeding 0 mV. Interestingly, brief inward currents occurred spontaneously that corresponded in size (10–20 pA) and duration (5–10 ms) to fast (glutamatergic) excitatory post-synaptic currents (EPSCs) that have been recorded in cortical neurons; this finding suggests that the differentiated iPS cells received functional synaptic inputs. As noted, the cell colonies formed dense fascicles of what appeared to be axons and indeed exhibited immune-positive staining for axon markers (Figs. 3, 4). To assess whether these structures contained competent axons, we applied stimulation pulses to the bundles at a distance of 200–300 μm from the colony edge while recording from a single cell body. When delivered under the control conditions, a stimulation pulse routinely evoked an EPSC with characteristics comparable to those occurring spontaneously (Fig. 4F).

These results strongly suggest that the nerve-like structures generated by the differentiated cells contained conducting axons with fully functional synapses. To further determine the functionality of the axons, we wondered whether the axons were capable of triggering antidromic spikes following the addition of the AMPA receptor antagonist CNQX. The EPSCs that are typically elicited by single pulses were not observed, but antidromic spikes were routinely recorded from the cell bodies (Fig. 4F). Collectively, these results demonstrate that the neuron-like cells differentiated from stem cells according to the procedures described developed the physiological characteristics of RGC neurons, including the production of nerve-like bundles that contained axons that both conducted spikes and formed glutamatergic synapses, suggesting that the differentiated neuron-like cells were functional.

Discussion

In this report, we have described a relatively straightforward and simple method for differentiating both hESCs and iPS cells into functional RGCs. We believe that the resulting streamlined protocol for producing high yields of RCGs from stem cells represents a significant advance in the development of RGC replacement therapy.

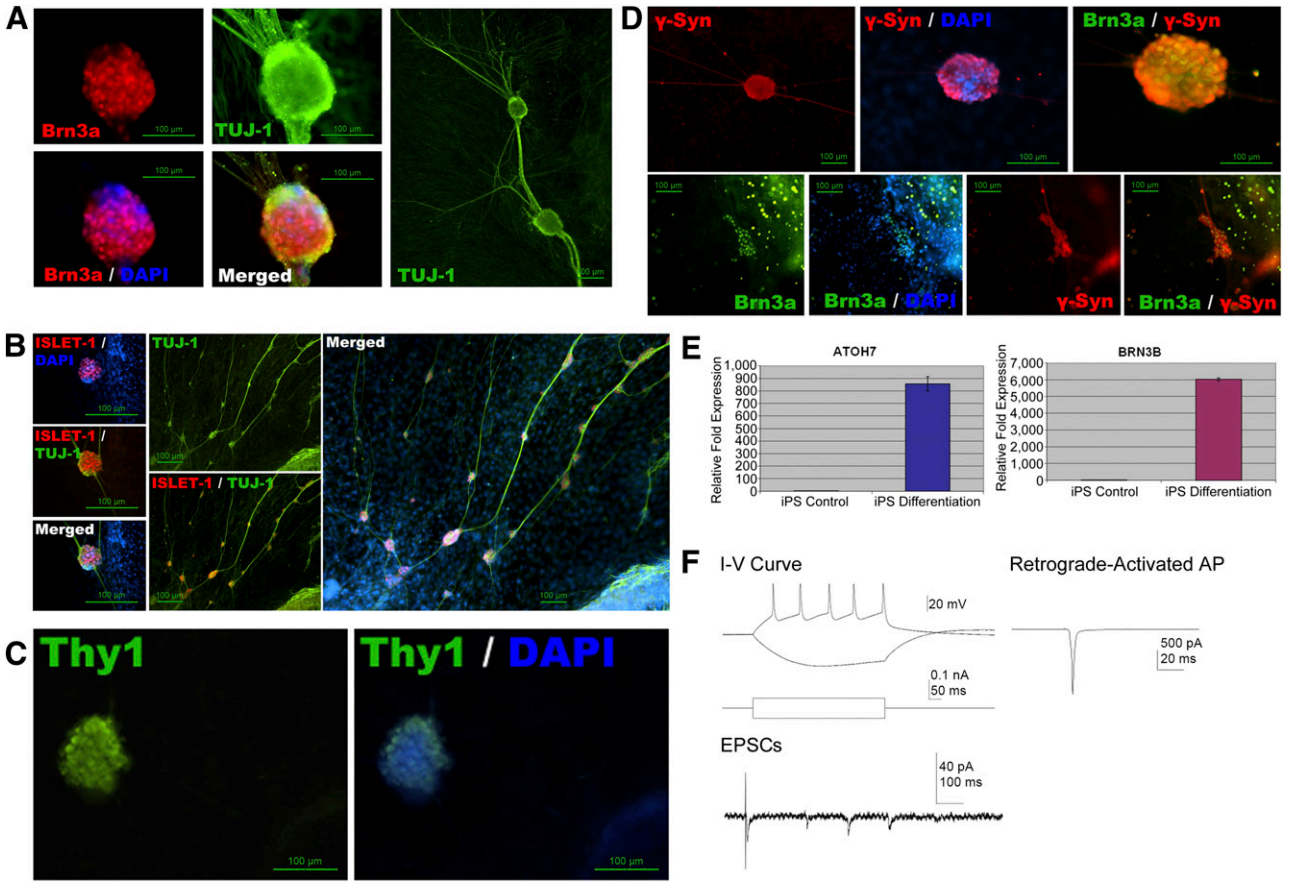

Figure 4. Differentiated human iPS cells express positive retinal ganglion cell (RGC) markers. **(A):** Expression of the neuronal marker TUJ1 and the RGC marker BRN3a following the application of a stepwise differentiation protocol to generate human iPS cells. BRN3a-positive cells exhibit fasciculated axons as RGCs in vivo. **(B):** Coexpression of TUJ1 and the RGC marker Islet-1 following the application of a stepwise differentiation protocol to generate human iPS cells. **(C):** Expression of THY-1 in differentiated human iPS cells. **(D):** Coexpression of the RGC markers γ-synuclein and BRN3a in differentiated human iPS cells. **(E):** Quantitative polymerase chain reaction analysis of ATOH7/Math5 and BRN3B in differentiated human iPS cells. Compared with the controls, the level of ATOH7/Math5 increased 857-fold and BRN3B increased 6,024-fold. **(F):** Electrophysiological analysis of differentiated RGCs. A resting membrane potential and emitted scattered spikes were recorded in the soma of cells when a current was supplied (top left); EPSCs evoked after a stimulus were applied to a distal axon-like structure (bottom left); an AP in the soma in presence of CNQX (right). Scale bars = 100 μm. Abbreviations: γ-Syn, γ-synuclein; AP, action potential; DAPI, 4′,6-diamidino-2-phenylindole; EPSC, excitatory postsynaptic current; iPS, induced pluripotent stem; I-V curve, current-voltage curve.

Several studies have reported and intended to generate retinal ganglion-like cells from embryonic stem cells and iPS cells [12, 28, 37, 38]. Using suspension culture in nonadherent culture dishes allows neurosphere formation. Cells can further differentiate into retinal progenitor epithelial cells and neural epithelial rosette-containing colonies. This was used to model early retinal development in hESCs and iPS cells [19]. Stepwise differentiation of stem cells into retinal cells has also been examined by other groups. After 4- to 5-month culture, hESCs can differentiate into retinal pigment epithelial and photoreceptor cells. To efficiently promote differentiation from RPCs into ganglion cells, we showed that DAPT was sufficient to promote the lineage differentiation to RGCs. Our protocol of differentiation of hESCs or iPS cells into RGC is much simpler compared with the protocol previously reported [24]. Our results indicate that Notch signaling plays an important role in stem cell differentiation and that it can be a potential target for clinical application.

Notch activity has been shown to be downregulated just before RGC differentiation [26]. DAPT can effectively inhibit the Notch signaling [27]. By mimicking this developmental process, we were able to differentiate iPS cells and hESCs into RGCs. Our stepwise differentiation protocol supports that Notch signaling plays a fundamental role in RGC differentiation, that DAPT is critical for inducing RGC differentiation from PAX6-positive/Rx-positive RPCs, and that Notch inhibitors might have therapeutic applications.

During vertebrate development, RGCs project their axons through the optic nerve into their targets within the brain [39]. RGCs process and convey signals from rod and cones directly to the visual centers in the brain [40]. This is a very complicated process. Studies using mouse models have shown that RGC development can be divided into three stages. First, ATOH7/Math5 is specifically required for competence, specification, and differentiation [41]. Pax6 is activated in the early competence stage and upregulates ATOH7/Math5. ATOH7/Math5 in turn plays an important role in RGC specification. ATOH7/Math5 performs this function in two ways. First, it activates genes specifically responsible for RGC differentiation. Second, ATOH7/Math5 represses expression of other bHLH transcription factors that are responsible for promoting other cell fates within the retina [41].

Our study also showed that hESCs and iPS cells can be differentiated into RGCs with similar efficiency. Because the use of hESCs in these therapies poses considerable ethical and technical challenges, the development of iPS cells represents a potential solution to the problems faced by hESC-based therapies; human iPS cells can be derived from readily obtainable adult cell types and are patient matched. Deriving iPS cells from patients with retinal degenerative diseases and differentiating the iPS cells into RGCs will facilitate our understanding of the molecular mechanisms behind specific cell-type differentiation and promote development of a potential cellular therapy.

This study holds great potential to apply cell transplant therapy in glaucoma, DOA, and LHON. All are caused by RGC loss. Because the majority of patients have significant RGC loss at diagnosis, medication would not be able to help them. Development of safe RGC transplantation techniques is needed to replace the lost cells. The retina could be an optimal model for investigation of stem cell therapy because the retina is most accessible for surgery and outcome monitoring. A previous study showed that visual restoration via a subretinal electronic prosthesis implies that even a severely degenerated retina may have the capacity for repair after cell replacement [42].

In order to translate our study to clinical applications, we will need to further test the efficacy of iPS cell differentiation in an animal model. There are a few animal models for glaucoma; however, not all models used for studying these diseases mimic the human disorders [43]. Mutations of OPA1 (optic atrophy 1) are responsible for the majority of DOA, thus the Opa1 knockout mouse could be a potential model. However, the phenotypes are not even seen until 18–20 months of age. Therefore the Opa1 knockout mouse may not be the best model for cell transplantation. Bst mice have a mutation in a ribosomal gene that causes almost complete loss of ganglion cells [44]. Pathologically, Bst mice could be used as an animal model for our future tests. We may have to determine whether RPCs injected intravenously could survive in vivo. In this case, the terminal differentiated cells may not be the best option because the axon could be as long as 2 cm. It would be more appropriate to transplant partially differentiated cells and coinject with DAPT. Therefore, the committed cells could continue to differentiate in vivo. Oral administration of DAPT might also promote the process.

Recently, embryonic RPCs were transplanted into adult mice. A significant number of E14.5 RPCs were able to differentiate into RGCs. However, RPCs contribute to restoring damaged optic nerves autonomously as well as nonautonomously [45]. The efficacy has yet to be determined. Transplantation of hESC-derived photoreceptors was able to restore visual function in a mouse model [46]. In addition, several studies in other conditions are encouraging. Stem cell therapy was used for amyotrophic lateral sclerosis, and it has been shown that stem cells provide neuroprotection in the animal models of ALS. Furthermore, the efficacy of neuroprogenitor cells-derived from iPS cells was tested, and respiratory function in these animal models of ALS was improved. Eleven independent studies showed slowed disease onset and progression, improved motor function, and significantly prolonged survival [47]. Spinal muscular atrophy is a motor neuron disease. In a mouse model of spinal muscular atrophy, spinal cord neural stem cells were transplanted into the spinal cords of mice. The transplanted cells developed into motor neurons, and the treated mice showed improved muscular function and increased lifespan. The major effect of neural stem cell transplantation is to improve the survival and function of the motor neurons. All of these conditions have the similar feature of RGC loss, suggesting cell replacement for RGCs could be a promising therapy [48].

Finally, eyes have much less immune rejection of transplanted cells. The survival of allogeneic porcine RPCs without immune suppression has been shown [49]. Previous study has supported the tolerance of RPCs as allografts, and a high level of rod photoreceptor development could be obtained from cultured RPCs following transplantation [49]. We may see immune rejection and will have to coinject the cells with immune-repressor or administer systemically. These points should be considered for future preclinical study.

Conclusion

We have developed a novel, stepwise chemical protocol to differentiate hES cells and iPS cells into functional RGCs. We found that a single chemical, DAPT, can induce PAX6/RX-positive stem cells to undergo differentiation into functional RGCs.

Acknowledgments

We thank the University of California (UC), Irvine, Stem Cell Core Facility for providing training and cell culture space. We are also grateful to Dr. Alexander Valencia, Dr. Robert Hufnagel, and the Huang laboratory for critically reading the manuscript. This work was partially supported by the UC Irvine Foundation, the Cincinnati Children's Hospital Research Foundation, and National Eye Institute (NEI) Grant 1R01EY018876. Research in the Huang laboratory is partially supported by the UC Irvine Foundation and by NEI Grant 1R01EY018876.

Author Contributions

H.R.: conception and design, collection and/or assembly of data, data analysis and interpretation, final approval of manuscript; Y.J.: collection and/or assembly of data, data analysis and interpretation; J.C.: data collection; G.L.: data analysis and interpretation, manuscript writing, final approval of manuscript; T.H.: conception and design, financial support, provision of study material, data analysis and interpretation, manuscript writing, final approval of manuscript.

Disclosure of Potential Conflicts of Interest

The authors indicate no potential conflicts of interest.

References

1 Quigley HA, Vitale S. Models of open-angle glaucoma prevalence and incidence in the United States. Invest Ophthalmol Vis Sci 1997; 38:83–91.

2 Medeiros FA, Alencar LM, Zangwill LM et al. Prediction of functional loss in glaucoma from progressive optic disc damage. Arch Ophthalmol 2009;127:1250–1256.

3 Votruba M, Aijaz S, Moore AT. A review of primary hereditary optic neuropathies. J Inherit Metab Dis 2003;26:209–227.

4 Carelli V, Ross-Cisneros FN, Sadun AA. Mitochondrial dysfunction as a cause of optic neuropathies. Prog Retin Eye Res 2004;23: 53–89.

5 Bette S, Schlaszus H, Wissinger B et al. OPA1, associated with autosomal dominant optic atrophy, is widely expressed in the human brain. Acta Neuropathol 2005;109:393–399.

6 Votruba M, Moore AT, Bhattacharya SS. Clinical features, molecular genetics, and pathophysiology of dominant optic atrophy. J Med Genet 1998;35:793–800.

7 Wallace DC. Mitochondrial genetics: A paradigm for aging and degenerative diseases? Science 1992;256:628–632.

8 Huang T, Santarelli R, Starr A. Mutation of OPA1 gene causes deafness by affecting function of auditory nerve terminals. Brain Res 2009;1300:97–104.

9 Wallace DC, Singh G, Lott MT et al. Mitochondrial DNA mutation associated with Leber's hereditary optic neuropathy. Science 1988;242: 1427–1430.

10 Dimos JT, Rodolfa KT, Niakan KK et al. Induced pluripotent stem cells generated from patients with ALS can be differentiated into motor neurons. Science 2008;321:1218–1221.

11 Brennand KJ, Simone A, Jou J et al. Modelling schizophrenia using human induced pluripotent stem cells. Nature 2011;473:221–225.

12 Parameswaran S, Balasubramanian S, Babai N et al. Induced pluripotent stem cells generate both retinal ganglion cells and photoreceptors: Therapeutic implications in degenerative changes in glaucoma and age-related macular degeneration. STEM CELLS 2010; 28:695–703.

13 Riesenberg AN, Le TT, Willardsen MI et al. Pax6 regulation of Math5 during mouse retinal neurogenesis. Genesis 2009;47:175–187.

14 Brown NL, Patel S, Brzezinski J et al. Math5 is required for retinal ganglion cell and optic nerve formation. Development 2001;128:2497–2508.

15 Yang Z, Ding K, Pan L et al. Math5 determines the competence state of retinal ganglion cell progenitors. Dev Biol 2003;264:240–254.

16 Ghiasvand NM, Rudolph DD, Mashayekhi M et al. Deletion of a remote enhancer near ATOH7 disrupts retinal neurogenesis, causing NCRNA disease. Nat Neurosci 2011;14:578–586.

17 Wang SW, Kim BS, Ding K et al. Requirement for math5 in the development of retinal ganglion cells. Genes Dev 2001;15:24–29.

18 Matter-Sadzinski L, Puzianowska-Kuznicka M, Hernandez J et al. A bHLH transcriptional network regulating the specification of retinal ganglion cells. Development 2005;132:3907–3921.

19 Meyer JS, Shearer RL, Capowski EE et al. Modeling early retinal development with human embryonic and induced pluripotent stem cells. Proc Natl Acad Sci USA 2009;106:16698–16703.

20 Mu X, Beremand PD, Zhao S et al. Discrete gene sets depend on POU domain transcription factor Brn3b/Brn-3.2/POU4f2 for their expression in the mouse embryonic retina. Development 2004;131:1197–1210.

21 Liu W, Khare SL, Liang X et al. All Brn3 genes can promote retinal ganglion cell differentiation in the chick. Development 2000;127: 3237–3247.

22 Nadal-Nicolás FM, Jiménez-López M, Sobrado-Calvo P et al. Brn3a as a marker of retinal ganglion cells: Qualitative and quantitative time course studies in naive and optic nerve-injured retinas. Invest Ophthalmol Vis Sci 2009;50:3860–3868.

23 Pan L, Deng M, Xie X et al. ISL1 and BRN3B co-regulate the differentiation of murine retinal ganglion cells. Development 2008;135: 1981–1990.

24 Surgucheva I, Weisman AD, Goldberg JL et al. Gamma-synuclein as a marker of retinal ganglion cells. Mol Vis 2008;14:1540–1548.

25 Barnstable CJ, Dräger UC. Thy-1 antigen: A ganglion cell specific marker in rodent retina. Neuroscience 1984;11:847–855.

26 Nelson BR, Gumuscu B, Hartman BH et al. Notch activity is downregulated just prior to retinal ganglion cell differentiation. Dev Neurosci 2006;28:128–141.

27 Crawford TQ, Roelink H. The notch response inhibitor DAPT enhances neuronal differentiation in embryonic stem cell-derived embryoid bodies independently of sonic hedgehog signaling. Dev Dyn 2007;236:886–892.

28 Chen M, Chen Q, Sun X et al. Generation of retinal ganglion-like cells from reprogrammed mouse fibroblasts. Invest Ophthalmol Vis Sci 2010;51:5970–5978.

29 Zhao R, Daley GQ. From fibroblasts to iPS cells: Induced pluripotency by defined factors. J Cell Biochem 2008;105:949–955.

30 Osakada F, Ikeda H, Sasai Y et al. Stepwise differentiation of pluripotent stem cells into retinal cells. Nat Protoc 2009;4:811–824.

31 Takahashi K, Yamanaka S. Induction of pluripotent stem cells from mouse embryonic and adult fibroblast cultures by defined factors. Cell 2006;126:663–676.

32 Esmailpour T, Huang T. TBX3 promotes human embryonic stem cell proliferation and neuroepithelial differentiation in a differentiation stage-dependent manner. STEM CELLS 2012;30:2152–2163.

33 Yarosh W, Barrientos T, Esmailpour T et al. TBX3 is overexpressed in breast cancer and represses p14 ARF by interacting with histone deacetylases. Cancer Res 2008;68: 693–699.

34 Liu J, Esmailpour T, Shang X et al. TBX3 over-expression causes mammary gland hyperplasia and increases mammary stem-like cells in an inducible transgenic mouse model. BMC Dev Biol 2011;11:65.

35 Jia Y, Gall CM, Lynch G. Presynaptic BDNF promotes postsynaptic long-term potentiation in the dorsal striatum. J Neurosci 2010;30: 14440–14445.

36 Itoh M, Nagafuchi A, Yonemura S et al. The 220-kD protein colocalizing with cadherins in non-epithelial cells is identical to ZO-1, a tight junction-associated protein in epithelial cells: cDNA cloning and immunoelectron microscopy. J Cell Biol 1993;121:491–502.

37 Jagatha B, Divya MS, Sanalkumar R et al. In vitro differentiation of retinal ganglion-like cells from embryonic stem cell derived neural progenitors. Biochem Biophys Res Commun 2009;380:230–235.

38 Zhao X, Liu J, Ahmad I. Differentiation of embryonic stem cells into retinal neurons. Biochem Biophys Res Commun 2002;297:177–184.

39 Isenmann S, Kretz A, Cellerino A. Molecular determinants of retinal ganglion cell development, survival, and regeneration. Prog Retin Eye Res 2003;22:483–543.

40 Ecker JL, Dumitrescu ON, Wong KY et al. Melanopsin-expressing retinal ganglion-cell photoreceptors: Cellular diversity and role in pattern vision. Neuron 2010;67:49–60.

41 Mu X, Fu X, Sun H et al. A gene network downstream of transcription factor Math5 regulates retinal progenitor cell competence and ganglion cell fate. Dev Biol 2005;280: 467–481.

42 Cramer AO, MacLaren RE. Translating induced pluripotent stem cells from bench to bedside: Application to retinal diseases. Curr Gene Ther 2013;13:139–151.

43 Bouhenni RA, Dunmire J, Sewell A et al. Animal models of glaucoma. J Biomed Biotechnol 2012;2012:692609.

44 Oliver ER, Saunders TL, Tarlé SA et al. Ribosomal protein L24 defect in belly spot and tail (Bst), a mouse Minute. Development 2004;131:3907–3920.

45 Cho JH, Mao CA, Klein WH. Adult mice transplanted with embryonic retinal progenitor cells: New approach for repairing damaged optic nerves. Mol Vis 2012;18:2658–2672.

46 Lamba DA, Gust J, Reh TA. Transplantation of human embryonic stem cell-derived photoreceptors restores some visual function in Crx-deficient mice. Cell Stem Cell 2009;4: 73–79.

47 Teng YD, Benn SC, Kalkanis SN et al. Multimodal actions of neural stem cells in a mouse model of ALS: A meta-analysis. Sci Transl Med 2012;4:165ra164.

48 Corti S, Nizzardo M, Nardini M et al. Neural stem cell transplantation can ameliorate the phenotype of a mouse model of spinal muscular atrophy. J Clin Invest 2008;118:3316–3330.

49 Klassen H, Kiilgaard JF, Warfvinge K et al. Photoreceptor differentiation following transplantation of allogeneic retinal progenitor cells to the dystrophic rhodopsin Pro347Leu transgenic pig. Stem Cells Int 2012;2012:939801.

See www.StemCellsTM.com for supporting information available online.